Available online at www.sciencedirect.com

ScienceDirect

Structural Integrity Procedia 00 (2019) 000–000

Structural Integrity Procedia

www.elsevier.com/locate/procedia

1st Virtual Conference on Structural Integrity – VCSI1

High fidelity numerical fracture mechanics assisted by RBF mesh morphing

Corrado Groth[a], Stefano Porziani[a], Andrea Chiappa[a], Edoardo Pompa[a,c], Riccardo Cenni[b], Matteo Cova[b], Gabriele D'Amico[c], Francesco Giorgetti[d], Carlo Brutti[a], Pietro Salvini[a], Michelle Rochette[e], Marco Evangelos Biancolini[a,*]

[a] *University of Rome "Tor Vergata", Via del Politecnico 1, Rome 00133, Italy*
[b] *SACMI Imola S.C. - Ceramic Engineering Department,Via Selice Provinciale, 17/A, Imola 40026, Italy*
[c] *Fusion for Energy, c/Josep Pla, n.2, Torres Diagonal Litoral, Edificio B3, E-08019, Barcelona, Spain*
[d] *Università degli Studi della Tuscia, Largo dell'Università, Viterbo 01100, Italy*
[e] *ANSYS France, 11 Avenue Albert Einstein, 69100 Villeurbanne, France*

Abstract

The study and design of cyclically loaded structures cannot neglect the evaluation of their fatigue behavior. Today numerical prediction tools allow adopting, in various industrial fields, refined and consolidated procedures for the assessment of cracked parts through analyses based on fracture mechanics. An high level of detail can be obtained through the use of well consolidated FEM methods, allowing an accurate and reliable calculation of the flaw Stress Intensity Factor (SIF) and its resulting prediction in terms of crack propagation. A challenging step for this computational workflow remains, however, the generation and update of the computational grid during crack evolution. It is in this context that radial basis functions (RBF) mesh morphing is emerging as a viable solution to replace the complex and time-consuming remeshing operation. The flaw front is updated, according to its propagation, by automatically deforming the numerical grid obtaining an evolutionary workflow suitable to be used for industrially-sized numerical meshes (many millions of nodes). A review of applications, obtained by exploiting FEA (Ansys Mechanical) and mesh morphing (RBF Morph) state of-the-art tools, is presented in this work. At first the proposed workflow is applied on a circular notched bar with a defect controlled by a two-parameters evolution. The same approach is then refined and demonstrated for a Multi Degree of Freedom (MDoF) case on the same geometry and on the vacuum vessel port stub from the fusion nuclear reactor Iter.

Keywords: 3-D cracks; Fatigue crack growth; SIF; RBF;

* Corresponding author. Tel.: +39 0672597124.
E-mail address: biancolini@ing.uniroma2.it

1. Introduction

To prevent sudden and unexpected breaks, that could lead to catastrophic failures and safety problems, it is required in several fields to study and predict the behaviour of crack growth. A component undergoing cyclic loading may, indeed, experience the generation of a crack that, generally, initiates on material surfaces in correspondence of singularities or stress concentrations. Subsequent fatigue cycles are responsible for the flaw evolution, that grows following preferential and higly stressed routes, until a critical size is reached. Given the level of danger linked with a sudden structural break, the engineering practice imposes a careful evaluation based on fracture mechanics theory, first theorized by the pioneeristic work of Griffith (1921), considering all the real materials as already containing cracks of some size. The evolution of the numerical prediction tools, and the increase of the computational power, allows today to adopt well consolidated and accurate finite element based methodologies, able to predict the evolution of the flaw by recurring to the concept of the Stress Intensity Factor (SIF). Methods commonly used in literature are the Boundary Element Method (BEM) (Mi and Aliabadi (1994), Cruse and Besuner (1975)), the Dual Boundary Element Method (DBEM) (Portela et al. (1993), Wang and Yao (2006)), the Finite Element Method (FEM) (Ingraffea (1977), Murakami and Keer (1993)) and the eXtended Finite Element Method (XFEM) (Pathak et al. (2013), Belytschko and Black (1999)). The vast majority of the advanced numerical methods, such as BEM, DBEM and XFEM require however a complex implementation stage in order to be commercially employed. By the other hand notable works by Carpinteri et al. (2003), Lin and Smith (1998) and Biancolini and Brutti (2002) demonstrated the use of commercial FEM methods to predict the flaw evolution by taking into account SIF values. These methods were employed also for a 3D crack evolution (Carter et al. (2000)), but an accurate modelling and simulation of the flaw evolution is still a difficult task given the requirements in terms of mesh quality. Citarella and Cricrì (2010) demonstrated that, although leading to similar results, FEM model solution times were always lower with respect to DBEM, at the cost of a time consuming remeshing algorithm difficult to be set up. An intrinsic characteristic of the FEM based methods in all the formulations cited, is indeed the requirement of a continuous remeshing to accomodate the numerical domain to a newly achieved crack geometry at each fatigue cycle. A very refined mesh near the flaw geometry must be assured, with the constraints of maintaining conformal the mesh near the crack front and the quarter point elements around the flaw to capture the singularity near the crack. Galland et al. (2011) demonstrated that an efficient crack growth simulation could be carried by exploiting mesh morphing. In this context radial basis functions (RBF) mesh morphing (De Boer et al. (2007a), Staten et al. (2011)) is emerging as a viable solution to replace the complex and time-consuming remeshing operation. RBF proved to be a reliable tool in several engineering fields (Biancolini (2017)) such as mesh morphing (De Boer et al. (2007a)), geometrical modelling (Kojekine et al. (2003)), shape optimization (Cella et al. (2017), Biancolini et al. (2016b)) including genetic or adjoint-based evolutionary methods (Groth et al. (2018)). It was also employed for steady (Biancolini et al. (2016a)) and unsteady (Di Domenico et al. (2018), Groth et al. (2019a)) Fluid Structure Interaction (FSI) problems, FEM results improvement (Chiappa et al. (2019b), Chiappa et al. (2019a)) and ice accretion studies (Groth et al. (2019b)). The RBF based mesh morphing tool can be employed also for the study of the crack growth, updating the flaw front by automatically morphing the mesh obtaining an evolutionary workflow suitable to be used for industrially sized grids.

Proposed procedure can be split in four main tasks for each iteration: the generation of a high fidelity numerical mesh respecting all the required features such as the use of quarter point elements and a satisfactory grid quality, the evaluation of the SIF values following the flaw front, the calculation of the displacements for each node by following the Paris-Ergdogan law (Paris and Erdogan (1963)), the mesh deformation by means of RBF mesh morphing employing the so achieved nodal displacements.

In this paper a review of fracture mechanics applications, tackled by synergically employing a commercially available FEM solver (ANSYS® Mechanical™) and an RBF morpher (RBF Morph) is shown. At first, as presented in Biancolini et al. (2018), proposed workflow was applied with a two Degrees of Freedom (DoF) model on a circular notched bar, following an analysis-then-update procedure. The same approach was then developed and demonstrated for a Multi Degree of Freedom (MDoF) case (Giorgetti et al. (2018)) and finally applied for the crack evolution on the vacuum vessel port stub from the fusion nuclear reactor Iter.

In the following sections at first a theoretical background will be given on RBF and on the crack propagation calculation. Problems and results for the three aforementioned cases will be then presented.

2. Theoretical background

2.1. Radial Basis Functions

Among the interpolation methods available for engineering calculation, RBF are a very powerful tool, able to determine the values of a scalar function starting from a discrete set of points (named source points) in the native space or in any of its subspaces. The interpolated values keep the exact ones of the function on the source points. The RBF are founded on a well stated theoretical background both from a mathematical (Buhmann (2000)) and application (Biancolini (2017)) point of view. To control the behavior of the function between the source points it is necessary to select the appropriate radial function and the domain where it is not zero valued (De Boer et al. (2007b)). RBF can be defined in a generic n dimensional space and are depending on the distance that, in the case of morphing, can be assumed as the Euclidean norm of the distance between two points in the space. Some of most common functions are shown in table 1. To define in full the RBF starting from passage information at source points, a

Table 1: Common RBF with global and local support.

Compactly supported RBF	Abbreviation	$\phi(\zeta)$, with $\zeta = \frac{r}{R}$
Wendland C^0	$C0$	$(1-\epsilon\zeta)^2$
Wendland C^2	$C2$	$(1-\epsilon\zeta)^4(4\epsilon\zeta+1)$
Wendland C^4	C4	$(1-\epsilon\zeta)^6(\frac{35}{3}\epsilon\zeta^2+6\epsilon\zeta+1)$
Globally supported RBF	**Abbreviation**	$\phi(r)$
Polyharmonic spline	*PHS*	r^n, n odd $r^n log(r)$, n even
Thin plate spline	*TPS*	$r^2 log(r)$
Multiquadric biharmonics	MQB	$\sqrt{a^2+(\epsilon r)^2}$
Inverse multiquadric biharmonics	IMQB	$\frac{1}{\sqrt{a^2+(\epsilon r)^2}}$
Quadric biharmonics	QB	$1+(\epsilon r)^2$
Inverse quadric biharmonics	IQB	$\frac{1}{1+(\epsilon r)^2}$
Gaussian biharmonics	GS	$e^{-\epsilon r^2}$

linear problem (Buhmann (2000)) must be solved in order to find system coefficients. Once the coefficients have been found the function at a given node of the mesh, being it inside (interpolation) or outside the domain (extrapolation), can be calculated according the radial summation centered at the probe position. Adopting such interpolation for the components of a deformation field it is then possible to define at known points the displacement in the space and then to retrieve it at mesh nodes, obtaining a mesh deformation that leaves unaltered the grid topology (Beckert and Wendland (2001), Biancolini (2012)).

The interpolation function is composed by the radial function ϕ and, in some situations, by a polynomial term h with a degree that depends on the kind of the chosen radial function which is added to assure uniqueness of the problem. If N is the total number of source points it can be written:

$$s(\mathbf{x}) = \sum_{i=1}^{N} \gamma_i \phi(||\mathbf{x} - \mathbf{x}_{k_i}||) + h(\mathbf{x}) \tag{1}$$

The passage of the RBF through source points and the imposing orthogonality conditions for the polynomial terms:

$$s(\mathbf{x}_{k_i}) = g_i, 1 \leq i \leq N \qquad \text{and} \qquad \sum_{i=1}^{N} \gamma_i p(\mathbf{x}_{k_i}) = 0 \tag{2}$$

for all the polynomials p of degree less or equal to polynomial h. A single interpolant exists if the basis is conditionally positive definite (Micchelli (1986)). If the degree is $m \leq 2$ (Beckert and Wendland (2001)) a linear polynomial can be used:

$$h(\mathbf{x}) = \beta_1 + \beta_2 x_1 + \beta_3 x_2 + ... + \beta_{n+1} x_n \tag{3}$$

The system 2 built to calculate coefficients and weights can be easily written in matrix form for an easy implementation:

$$\begin{bmatrix} \mathbf{M} & \mathbf{P} \\ \mathbf{P}^T & \mathbf{0} \end{bmatrix} \begin{Bmatrix} \boldsymbol{\gamma} \\ \boldsymbol{\beta} \end{Bmatrix} = \begin{Bmatrix} \mathbf{g} \\ \mathbf{0} \end{Bmatrix} \tag{4}$$

Where $\mathbf{g}$ is is the vector of known terms for each source point and $\mathbf{M}$ is the interpolation matrix with the radial function transformed distances between source points:

$$M_{ij} = \phi(\|\mathbf{x}_{k_i} - \mathbf{x}_{k_j}\|), 1 \leq i \leq N, 1 \leq j \leq N \tag{5}$$

$\mathbf{P}$ is the constraint matrix resulting from the orthogonality conditions:

$$\mathbf{P} = \begin{pmatrix} 1 & x_{k_1} & y_{k_1} & z_{k_1} \\ 1 & x_{k_2} & y_{k_2} & z_{k_2} \\ \vdots & \vdots & \vdots & \\ 1 & x_{k_N} & y_{k_N} & z_{k_N} \end{pmatrix} \tag{6}$$

The system 4 is solved considering as known terms the three components of the deformation field. Once the RBF weights and polynomial coefficients of the system have been obtained, displacement values for the three directions can be obtained at a given $\mathbf{x}$ point as:

$$\begin{cases} S_x(\mathbf{x}) = \sum_{i=1}^{N} \gamma_i^x \phi(\|\mathbf{x} - \mathbf{x}_{k_i}\|) + \beta_1^x + \beta_2^x x_1 + \beta_3^x x_2 + \beta_4^x x_n \\ S_y(\mathbf{x}) = \sum_{i=1}^{N} \gamma_i^y \phi(\|\mathbf{x} - \mathbf{x}_{k_i}\|) + \beta_1^y + \beta_2^y x_1 + \beta_3^y x_2 + \beta_4^y x_n \\ S_z(\mathbf{x}) = \sum_{i=1}^{N} \gamma_i^z \phi(\|\mathbf{x} - \mathbf{x}_{k_i}\|) + \beta_1^z + \beta_2^z x_1 + \beta_3^z x_2 + \beta_4^z x_n \end{cases} \tag{7}$$

2.2. Crack Propagation

The propagation of a crack with a Multiple Degrees of Freedom (MDOF) model is a complex task and different mathematical aspects need to be managed. The first topic concerns the values of displacement, related to the flaw

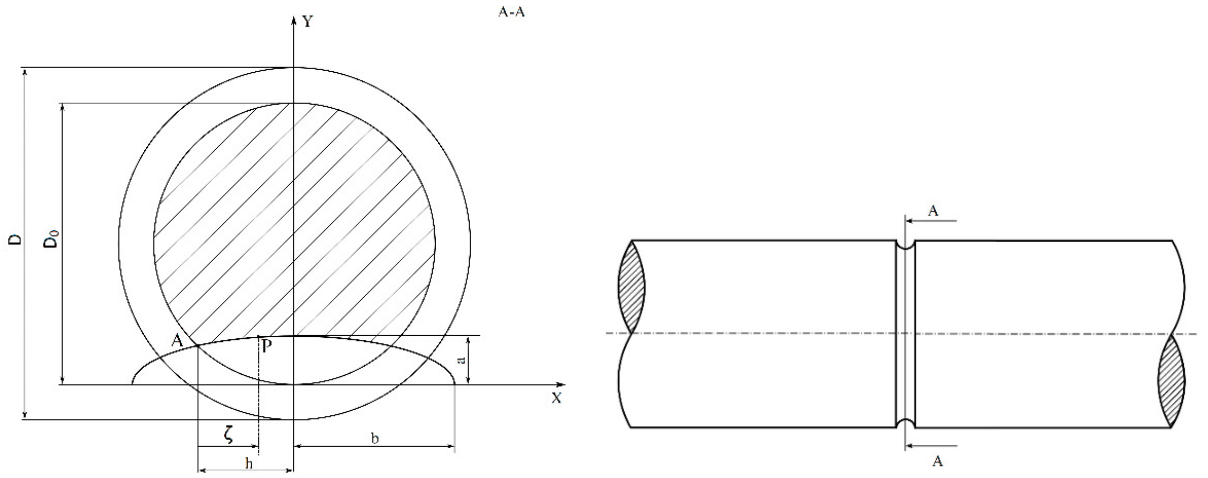

Fig. 1: Left: geometry nomenclature; right: circular notched bar.

growth, that have to be imposed to the nodes of crack front, by means of mesh morphing. In particular the local increment Δa_i of the $i-th$ node, is calculated using a Euler integration algorithm (Paris and Erdogan (1963)) based on the Paris-Erdogan law (Equation 8).

$$\frac{da}{dN} = C\Big(\Delta K\Big)^m \tag{8}$$

In which C and m are material properties. Making use of the effective Stress Intensity Factors (SIFs), extracted from the $j-th$ Finite Element Analysis (FEA), and defining a starting value for Δa_{max}, it is possible to evaluate the growth increment of each node of the front normalized with respect to $\Delta K^{(j)}_{max}$:

$$\Delta a^{(j)}_i = \left(\frac{\Delta K^{(j)}_i}{\Delta K^{(j)}_{max}}\right)^m \Delta a^{(j)}_{max} \tag{9}$$

In addition, the maximum crack growth increment $\Delta a^{(j)}_{max}$, with the corresponding maximum SIFs $\Delta K^{(j)}_{max}$ are introduced in the following formula for the evaluation of the loading cycles:

$$\Delta N^j = \frac{\Delta a^{(j)}_{max}}{C(\Delta K^{(j)}_{max})^m} \tag{10}$$

3. Applications

3.1. 2 DoF notched bar

Proposed workflow is first implemented, as shown by Biancolini et al. (2018), in Ansys® Workbench™for a simple circular notched bar, employing the same geometry explored by Carpinteri et al. (2003) in their work.

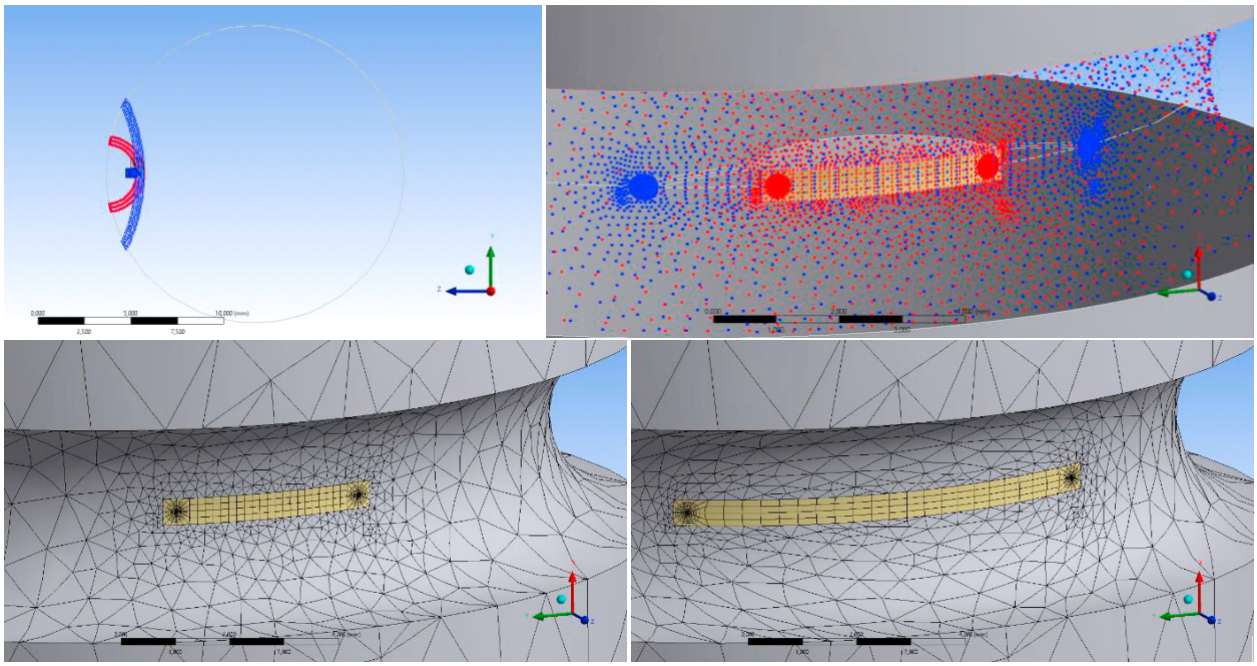

Fig. 2: Above: RBF setup for the crack morphing; bottom: baseline and morphed mesh.

In Figure 1 the round bar with notch radius ρ equal to 2 mm is shown. Other measures, complying with the already cited work by Carpinteri, are $D_0 = 16mm$ and $D = 20mm$, maintaining a bar lenght of $80mm$ in order to extinguish any boundary effect, and a tensile load of $30kN$. The crack geometry was added to the bar by taking advantage of the fracture mechanics tool (FT) implemented in Workbench^{TM}, that allows to insert a given crack geometry by locally modifying a pre-existing mesh.

After a mesh convergence test with respect to the notch concentration factor (K_t computed equal to 2.214, comparing to a theoretical reference of 2.2 from Pilkey and Pilkey (2008)), a first benchmarking was executed on a predefined set of crack geometries to test the reliability of the numerical results obtained by RBF mesh morphing comparing them to a full remeshing. The employed computational grid, which mesh count is 29k elements and is composed of 10-nodes iso-parametric tetrahedrons, was modelled employing quarter-point wedges around the crack front in order to correctly capture the stress singularity for the SIF calculation.

The RBF setup employed to morph the baseline crack is shown in fig. 2. Crack deformation was achieved by controlling three lines: one following the crack and two following the already mentioned set of quarter-point wedge elements around the defect on a perpendicular plane with respect to the notch. This strategy was followed in order to accurately deform the crack while maintaining a proper aspect ratio of the wedge elements around of it to guarantee a satisfactory SIF calculation.

Several runs were carried changing the crack aspect ratio, defined as $\alpha = a/b$, under a tensile static load of $30kN$. To compare results to literature data, the curvilinear abscissa and the resulting SIF were normalized by following these relations:

$$\zeta^* = \frac{\zeta}{h} \quad , \quad K_I^* = \frac{K_I}{\sigma_F \sqrt{\pi a}} \quad \text{where} \quad \sigma_F = \frac{4F}{\pi D_0^2} \tag{11}$$

In fig. 3 left, the comparison of the SIF values along the normalized curvilinear abscissa is shown between the geometries obtained with a morphing action or by inserting cracks in the mesh using the FT tool. On the right image

are shown the dimensionless SIF values obtained with mesh morphing varying the crack aspect ratio, results compare very good with those shown in Carpinteri et al. (2003).

Having demonstrated the ability of RBF morphing to adapt the crack shape to a new geometry, a crack growth simulation was carried, employing the Paris-Erdogan law as shown in eq. (8) taking, as material dependent coefficients, the values suggested by RCC-MR (2007). By assuming a fatigue load from zero, was taken into account as SIF the K_I, mode 1 of loading, as suggested by Anderson (2005). Instead of evaluating the SIF for each node at each iteration, a 2-DoF model controlling the two surface points and the deepest point on the symmetry axis was put into place, having noticed that the maximum values of SIF are available on the near-surface points, while the lower one on the deepest point along the symmetry. In fig. 4 the three controlled points are shown on the geometry, referencing with A and C the two near-surface points and with B the in-depth point on the symmetry. In Table 2 the resulting parameters of the accretion are shown, together with the equivalent number of cycles and with the evolution of the flaw in Figure 4.

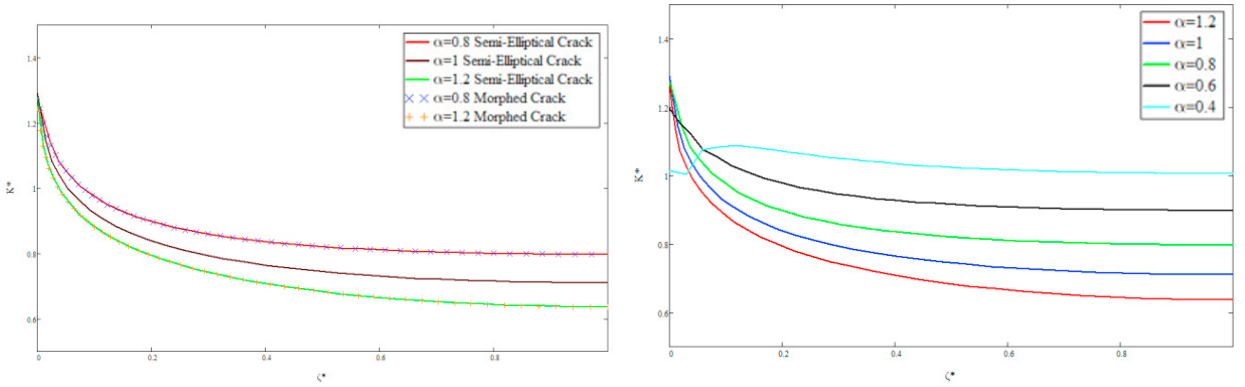

Fig. 3: Left: Normalized SIF comparison between remeshed and morphed cracks; right: normalized SIF for cracks inserted with FT.

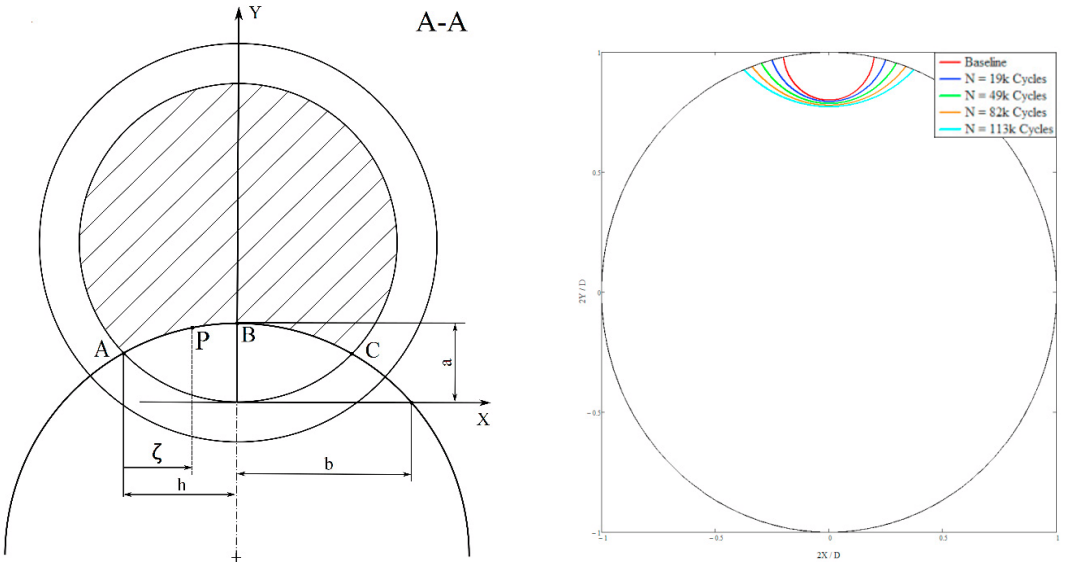

Fig. 4: Left: controlled crack points on the geometry; right: crack development.

Table 2: Dimensional parameters of the evolving crack and relative number of cycles.

a [mm]	b [mm]	α []	N_{cyc} [kCycles]	SIF_{max} $\left[MPa \cdot \sqrt{mm}\right]$	SIF_{min} $\left[MPa \cdot \sqrt{mm}\right]$
1.60	1.60	1.00	0	433.75	238.47
1.65	2.15	0.76	18.83	385.89	265.31
1.71	2.56	0.63	48.90	377.55	288.93
1.77	3.27	0.54	81.71	381.82	310.61
1.82	3.48	0.47	113.08	0	0

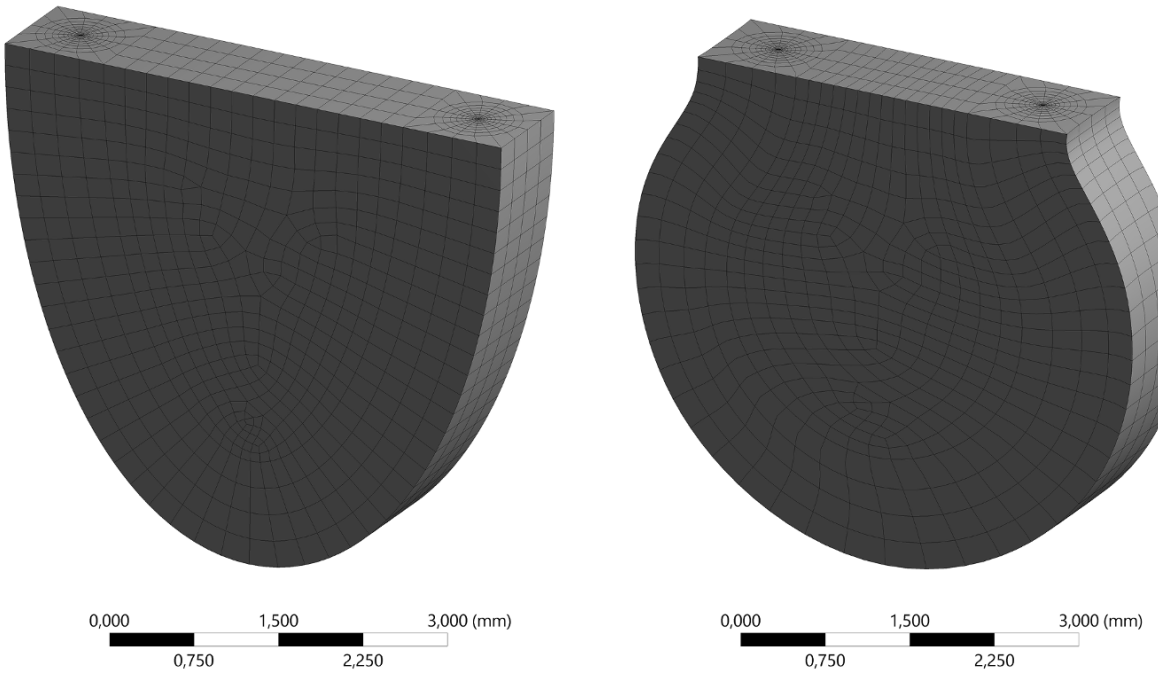

Fig. 5: Left: mesh obtained using the Ansys FT; right: omega shaped mesh geometry after RBF morphing.

3.2. MDoF crack propagation

Proposed method, refined for a three dimensional problem, was also applied for the propagation study of a crack in a MDoF case, evaluating its development from the free surface appearance to its complete evolution. An under-surface crack has indeed a circular conformation until the breakout. Once reached the surface, the crack geometry assumes an omega shape that, during its evolution, transforms into a semielliptical configuration as demonstrated by Dai et al. (1998). In this study, the MDOF model was employed to demonstrate that a three dimensional flaw evolves from an omega shape to a semielliptical one during its development. The starting omega shaped crack mesh was at first obtained by deforming by means of RBFs the mesh representing the semielliptical final configuration, in order to have a fair term of comparison in term of geometries: the final flaw evolved shape can be compared, after the study, with the one employed as a starting configuration before the initial morphing. The Ansys FT was used once again to generate the semielliptical crack employed as a starting point.

In Figure 5 the baseline geometry obtained with the FT, and goal of this study, is shown on the left. On the right the semielliptical mesh obtained after the morphing action is also shown. The RBF setup employed to obtain such a deformation consisted in controlling directly the crack front and by smoothly prescribing a similar deformation to the boundaries of the quarter node wedges wrapping the crack. In Figure 7, on the right, the original and final positions of

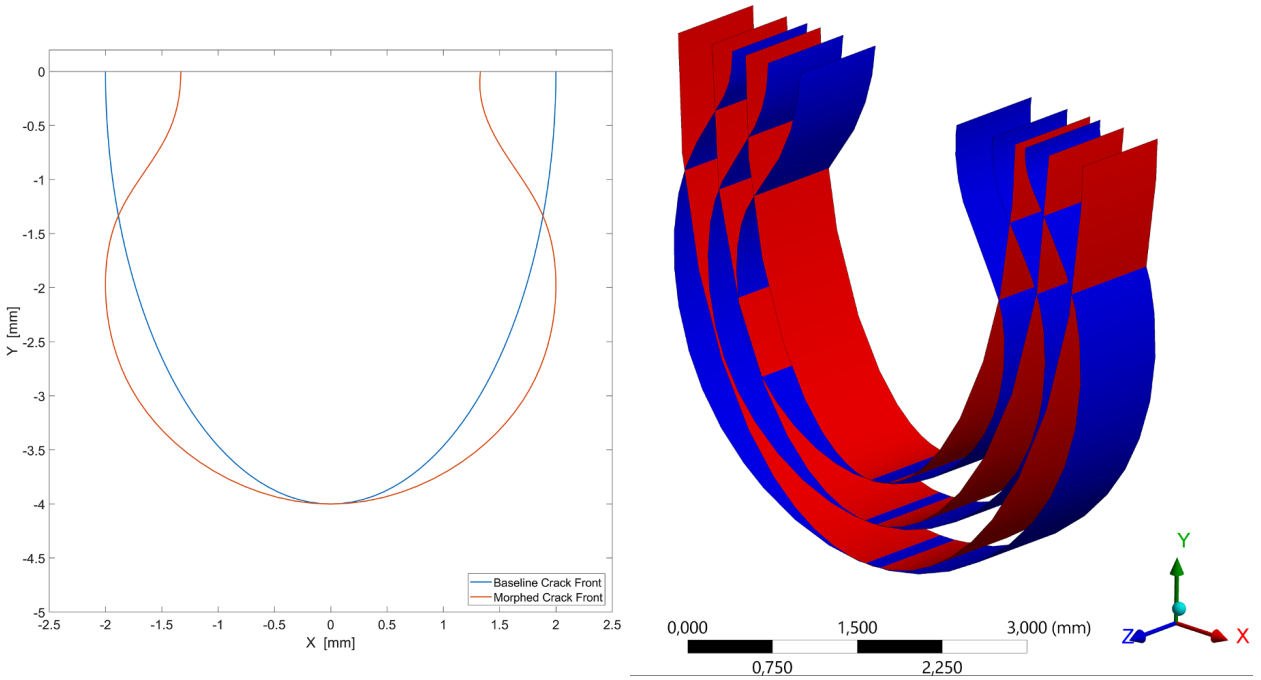

Fig. 6: Left: omega-shaped and semielliptical geometries; right: semiellipltical and omega-shaped surfaces employed for morphing.

such sets are displayed in red and blue respectively. To generate the morphing setup, RBF source points were seeded on the red surfaces and projected onto the blue ones.

To control the crack evolution, starting from the right configuration in Figure 5, the Paris-Erdogan equation shown in 8 was employed as in the 2 DoF case. Displacements were computed using the SIF for each node, applying them normally with respect to the crack front. The normal displacements for each node were obtained by computing the weighted average of the normal vector for each segment reaching the node:

$$\overrightarrow{Nn_i} = \frac{\overrightarrow{Ns_i} \cdot Ls_i + \overrightarrow{Ns_{(i+1)}} \cdot Ls_{(i+1)}}{Ls_i + Ls_{(i+1)}} \tag{12}$$

where $\overrightarrow{Nn}$ is the displacement direction on the i^{th} node, and $\overrightarrow{Ns_i}$ and $\overrightarrow{Ns_{i+1}}$ are the normal components of the previous and subsequent segment respectively.

3.3. Iter vacuum vessel port stub

To finally demonstrate its capability to tackle complex industrial application, the method was applied to the evolution of two initial elliptical cracks in one of the port stub of the ITER Vacuum Vessel (VV) Sector 5, and results have been compared to the ones obtained by the assessment performed in accordance to RCC-MR nuclear code RCC-MR (2007). The work demonstrated the accuracy of the proposed procedure, while underlying the important differences in the shape evolution when using a 2 Dof or a MDoF model.

After a first structural analysis, in which the most favorable location for the crack generation and evolution has been identified as the corner smoothed edge of the port stub (Figure 8b), the propagation analysis has been carried out with the same setup both for the 2DoF model assessment foreseen by the nuclear codes and the MDoF.

The full load spectrum, i.e. the contribution of each load condition and number of cycles (including gravity, normal operation condition, major disruption and magnet fast discharge, as detailed for the MLC III-4C 2 in ITER Vacuum

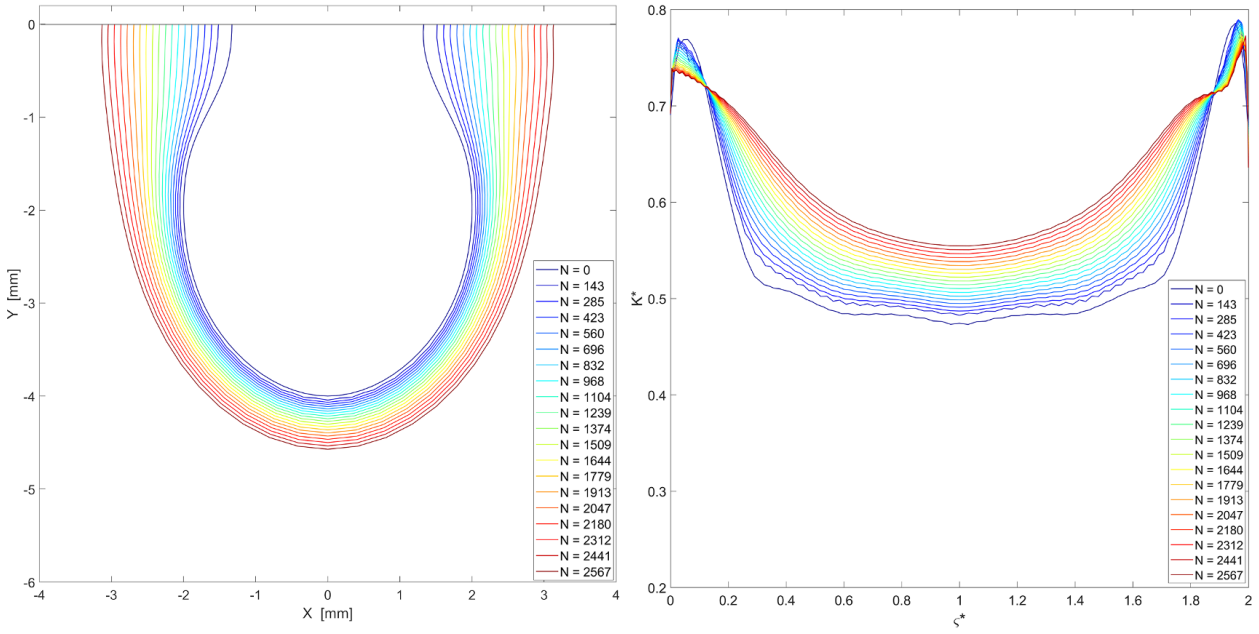

Fig. 7: Left: crack evolution with respect to cycles; right: SIF values on the nondimensional curvilinear abscissa.

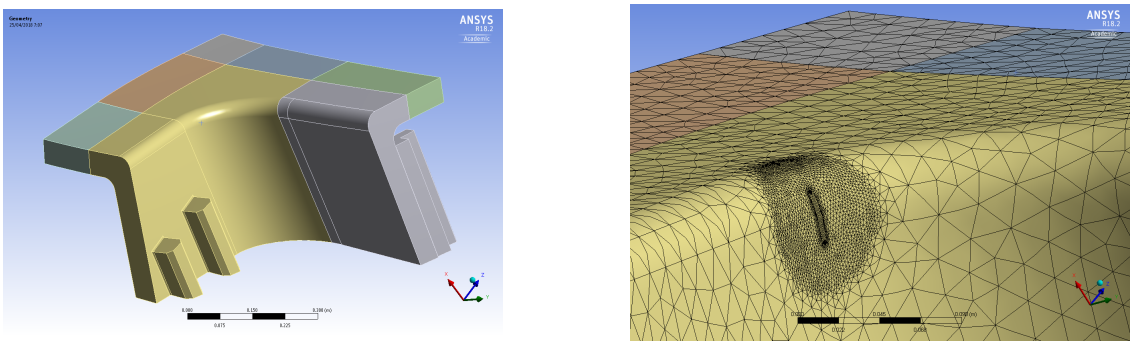

(a) VV port stub sub model

(b) Detail of crack location

Fig. 8

Vessel Load Specification ITER (2007)), has been taken into account by the use of Miner rule for cumulative damage, defining an equivalent cyclic load and number of cycles producing the same damage in the flawed part.

As shown in Figure 9, where the evolution of the crack half width has been plotted against crack depth for the estimated life of 7280 cycles, the comparison of the crack geometrical parameters demonstrates that the two models lead to very similar results.

According to the peak fracture parameters, divided for their critical value and plotted against the number of cycles in Figure 10a and Figure 10b, there is a good agreement between the two models.

Since the crack is close to the smoothed edge of the port stub, the fracture parameters curves are not symmetric with respect to the elliptical crack minor axis (Figure 11b). In this condition the MDOF model describes with a more accurate level of detail the asymmetric evolution of the crack, which lead to a higher growth of the crack side close to the smoothed edge (Figure 11a), while the crack of the 2DOF model remains elliptical during its evolution.

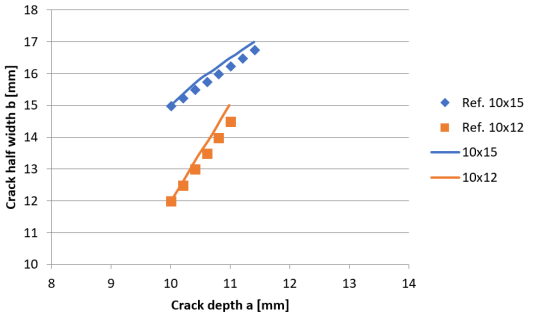

Fig. 9: Elliptical cracks shape evolution: comparison with 2DOF model

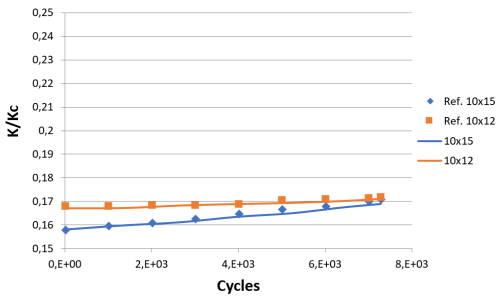

(a) Evolution of peak SIF ratio

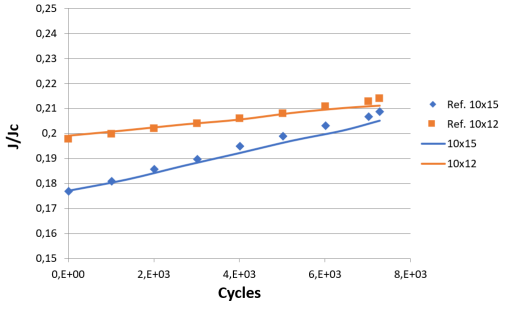

(b) Evolution of peak J integral ratio

Fig. 10

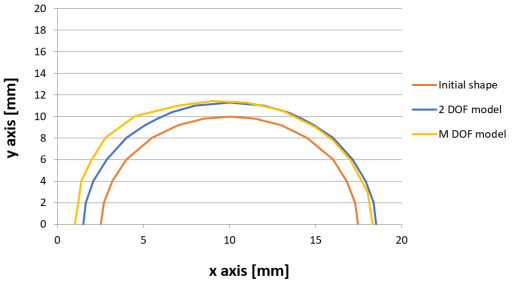

(a) Comparison of the shape evolution of the elliptical crack 10x15 after 7280 cycles

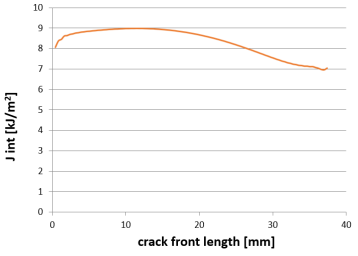

(b) Trend of J integral along the crack length

Fig. 11

4. Conclusions

In this paper a review of applications tackling numerical fracture machanics, obtained by exploiting FEA (Ansys Mechanical) and mesh morphing (RBF Morph) state of-the-art tools, was given. Two different approaches were presented in order to study the flaw evolution by deforming the computational grid according to the Paris-Erdogan law using Radial Basis Functions (RBF). At first a 2 degree of freedom model was implemented, guiding the in-plane crack development by using two stress intensity factor (SIF) values, one on the in-depth point on the symmetry and one on the surface. This model was then improved by evaluating the SIF along the crack profile, guiding its evolution by projecting the displacements along the crack normals. These two approaches were at first demonstrated on a notched

bar and compared to literature results, then applied to the vacuum vessel port stub from the fusion nuclear reactor Iter, demonstrating the ability of the proposed methods of tackling the evolution of a crack in a three dimensional problem.

5. Acknowledgement

The present work was developed within the research project "SMART MAINTENANCE OF INDUSTRIAL PLANTS AND CIVIL STRUCTURES BY 4.0 MONITORING TECHNOLOGIES AND PROGNOSTIC APPROACHES - MAC4PRO ", sponsored by the call BRIC-2018 of the National Institute for Insurance against Accidents at Work - INAIL.

References

Anderson, T.L., 2005. Fracture mechanics: fundamentals and applications. CRC press.

Beckert, A., Wendland, H., 2001. Multivariate interpolation for fluid-structure-interaction problems using radial basis functions. Aerospace Science and Technology 5, 125–134. doi:10.1016/S1270-9638(00)01087-7.

Belytschko, T., Black, T., 1999. Elastic crack growth in finite elements with minimal remeshing. International journal for numerical methods in engineering 45, 601–620.

Biancolini, M., Brutti, C., 2002. A numerical technique to study arbitrary shaped cracks growing in notched elements. International Journal of Computer Applications in Technology 15, 176–185.

Biancolini, M., Chiappa, A., Giorgetti, F., Porziani, S., Rochette, M., 2018. Radial basis functions mesh morphing for the analysis of cracks propagation. Procedia Structural Integrity 8, 433–443.

Biancolini, M.E., 2012. Mesh Morphing and Smoothing by Means of Radial Basis Functions (RBF), in: Handbook of Research on Computational Science and Engineering. IGI Global. volume I, pp. 347–380. doi:10.4018/978-1-61350-116-0.ch015.

Biancolini, M.E., 2017. Fast radial basis functions for engineering applications. Springer.

Biancolini, M.E., Cella, U., Groth, C., Genta, M., 2016a. Static Aeroelastic Analysis of an Aircraft Wind-Tunnel Model by Means of Modal RBF Mesh Updating. Journal of Aerospace Engineering 29. URL: https://www.scopus.com/inward/record.uri?eid=2-s2.0-84991573517{&}doi=10.1061{%}2F{%}28ASCE{%}29AS.1943-5525.0000627{&}partnerID=40{&}md5=548c1052f529a7ec2d9da6b198b79c8e, doi:10.1061/(ASCE)AS.1943-5525.0000627.

Biancolini, M.E., Costa, E., Cella, U., Groth, C., Veble, G., Andrejašič, M., 2016b. Glider fuselage-wing junction optimization using CFD and RBF mesh morphing. Aircraft Engineering and Aerospace Technology 88, 740–752. URL: https://www.scopus.com/inward/record.uri?eid=2-s2.0-84991698492{&}doi=10.1108{%}2FAEAT-12-2014-0211{&}partnerID=40{&}md5=7ec910e5bb8815fd37a33abf0ae3f02d, doi:10.1108/AEAT-12-2014-0211.

Buhmann, M.D., 2000. Radial basis functions. Acta Numerica 2000 9, S0962492900000015. doi:10.1017/S0962492900000015.

Carpinteri, A., Brighenti, R., Spagnoli, A., Vantadori, S., 2003. Fatigue growth of surface cracks in notched round bars, in: FCP2003.

Carter, B., Wawrzynek, P., Ingraffea, A., 2000. Automated 3-d crack growth simulation. International journal for numerical methods in engineering 47, 229–253.

Cella, U., Groth, C., Biancolini, M., 2017. Geometric parameterization strategies for shape optimization using RBF mesh morphing. doi:10.1007/978331945781954.

Chiappa, A., Groth, C., Biancolini, M.E., 2019a. Improvement of 2D finite element analysis stress results by radial basis functions and balance equations. International Journal of Mechanics 13, 90–99. URL: https://www.scopus.com/inward/record.uri?eid=2-s2.0-85071857099{&}partnerID=40{&}md5=966612b6d774c3980a40dfcef3b408ea.

Chiappa, A., Salvini, P., Brutti, C., Biancolini, M.E., 2019b. Upscaling 2d finite element analysis stress results using radial basis functions. Computers & Structures 220, 131–143.

Citarella, R., Cricrì, G., 2010. Comparison of dbem and fem crack path predictions in a notched shaft under torsion. Engineering Fracture Mechanics 77, 1730–1749.

Cruse, T.A., Besuner, P., 1975. Residual life prediction for surface cracks in complex structural details. Journal of Aircraft 12, 369–375.

Dai, D., Hills, D., Härkegard, G., Pross, J., 1998. Simulation of the growth of near-surface defects. Engineering fracture mechanics 59, 415–424.

De Boer, A., Van der Schoot, M., Bijl, H., 2007a. Mesh deformation based on radial basis function interpolation. Computers & structures 85, 784–795.

De Boer, A., van der Schoot, M.S., Bijl, H., 2007b. Mesh deformation based on radial basis function interpolation. Computers and Structures 85, 784–795. doi:10.1016/j.compstruc.2007.01.013.

Di Domenico, N., Groth, C., Wade, A., Berg, T., Biancolini, M.E., 2018. Fluid structure interaction analysis: Vortex shedding induced vibrations, in: Procedia Structural Integrity, pp. 422–432. URL: https://www.scopus.com/inward/record.uri?eid=2-s2.0-85051665685{&}doi=10.1016{%}2Fj.prostr.2017.12.042{&}partnerID=40{&}md5=153ba0660d813a551cc3a0a3032c8357, doi:10.1016/j.prostr.2017.12.042.

Galland, F., Gravouil, A., Malvesin, E., Rochette, M., 2011. A global model reduction approach for 3d fatigue crack growth with confined plasticity. Computer Methods in Applied Mechanics and Engineering 200, 699–716.

Giorgetti, F., Cenni, R., Chiappa, A., Cova, M., Groth, C., Pompa, E., Porziani, S., Biancolini, M.E., 2018. Crack Propagation Analysis of Near-Surface Defects with Radial Basis Functions Mesh Morphing, in: Procedia Structural Integrity, pp. 471–

478. URL: https://www.scopus.com/inward/record.uri?eid=2-s2.0-85064674094{&}doi=10.1016{%}2Fj.prostr.2018.11.071{&}partnerID=40{&}md5=21232f0224be249b8e0348e7ae30a519, doi:10.1016/j.prostr.2018.11.071.

Griffith, A.A., 1921. Vi. the phenomena of rupture and flow in solids. Philosophical transactions of the royal society of london. Series A, containing papers of a mathematical or physical character 221, 163–198.

Groth, C., Cella, U., Costa, E., Biancolini, M., 2019a. Fast high fidelity CFD/CSM fluid structure interaction using RBF mesh morphing and modal superposition method. Aircraft Engineering and Aerospace Technology 91, 893–904. URL: https://doi.org/10.1108/AEAT-09-2018-0246, doi:10.1108/AEAT-09-2018-0246.

Groth, C., Chiappa, A., Biancolini, M., 2018. Shape optimization using structural adjoint and rbf mesh morphing. Procedia Structural Integrity 8, 379–389.

Groth, C., Costa, E., Biancolini, M.E., 2019b. RBF-based mesh morphing approach to perform icing simulations in the aviation sector. Aircraft Engineering and Aerospace Technology 91, 620–633. URL: https://www.scopus.com/inward/record.uri?eid=2-s2.0-85062104000{&}doi=10.1108{%}2FAEAT-07-2018-0178{&}partnerID=40{&}md5=935623d05197b59add119d6af753c57e, doi:10.1108/AEAT-07-2018-0178.

Ingraffea, A., 1977. Nodal grafting for crack propagation studies. International Journal for Numerical Methods in Engineering 11, 1185–1187.

ITER, 2007. Iter vacuum vessel load specification.

Kojekine, N., Hagiwara, I., Savchenko, V., 2003. Software tools using CSRBFs for processing scattered data. Computers and Graphics (Pergamon) 27, 311–319. doi:10.1016/S0097-8493(02)00287-X.

Lin, X., Smith, R., 1998. Fatigue growth simulation for cracks in notched and unnotched round bars. International Journal of Mechanical Sciences 40, 405–419.

Mi, Y., Aliabadi, M., 1994. Three-dimensional crack growth simulation using bem. Computers & Structures 52, 871–878.

Micchelli, C.A., 1986. Interpolation of scattered data: Distance matrices and conditionally positive definite functions. Constructive Approximation 2, 11–22. doi:10.1007/BF01893414.

Murakami, Y., Keer, L., 1993. Stress intensity factors handbook, vol. 3. Journal of Applied Mechanics 60, 1063.

Paris, P., Erdogan, F., 1963. A critical analysis of crack propagation laws .

Pathak, H., Singh, A., Singh, I.V., 2013. Fatigue crack growth simulations of 3-d problems using xfem. International Journal of Mechanical Sciences 76, 112–131.

Pilkey, W.D., Pilkey, D.F., 2008. Peterson's stress concentration factors. John Wiley & Sons.

Portela, A., Aliabadi, M., Rooke, D.P., 1993. Dual boundary element incremental analysis of crack propagation. Computers & Structures 46, 237–247.

RCC-MR, D., 2007. Construction rules for mechanical components of nuclear installations. AFCEN: Paris, France .

Staten, M.L., Owen, S.J., Shontz, S.M., Salinger, A.G., Coffey, T.S., 2011. A comparison of mesh morphing methods for 3d shape optimization, in: Proceedings of the 20th international meshing roundtable. Springer, pp. 293–311.

Wang, P., Yao, Z., 2006. Fast multipole dbem analysis of fatigue crack growth. Computational Mechanics 38, 223–233.